SPECIAL ISSUE - ORIGINAL ARTICLE

Space–time network connectivity and cortical activations preceding spike wave discharges in human absence epilepsy: a MEG study

Disha Gupta · Pauly Ossenblok · Gilles van Luijtelaar

Abstract To describe the spatial and temporal profiles of connectivity networks and sources preceding generalized spike-and-wave discharges (SWDs) in human absence epilepsy. Nonlinear associations of MEG signals and cluster indices obtained within the framework of graph theory were determined, while source localization in the frequency domain was performed in the low frequency bands with dynamic imaging of coherent sources. The results were projected on a three-dimensional surface rendering of the brain using a semi-realistic head model and MRI images obtained for each of the five patients studied. An increase in clustering and a decrease in path length preceding SWD onset and a rhythmic pattern of increasing and decreasing connectivity were seen during SWDs. Beamforming showed a consistent appearance of a low frequency frontal cortical source prior to the first generalized spikes. This source was preceded by a low frequency occipital source. The changes in the connectivity networks with the onset of SWDs suggest a pathologically predisposed state towards synchronous seizure networks with increasing connectivity from interictal to preictal and ictal state, while the occipital and frontal low frequency early preictal sources demonstrate that SWDs are not suddenly arising but gradually build up in a dynamic network.

D. Gupta · G. van Luijtelaar
Donders Centre for Cognition, Institute for Brain Cognition and Behaviour, Radboud University Nijmegen, Montessorilaan 3, 6525 HR Nijmegen, The Netherlands

P. Ossenblok (✉)
Department of Clinical Physics, Epilepsy Center
Kempenhaeghe, Sterkselseweg 65, 5591 VE Heeze,
The Netherlands
e-mail: ossenblokp@kempenhaeghe.nl

1 Introduction

High inter-hemispheric synchronization of 3 Hz spike-and-wave discharges (SWDs) in both hemispheres of the brain, associated with impaired consciousness called *absence seizures* have been suggested to be *generalized* [20]. These seizures are prevalent in a form of idiopathic generalized epilepsy, previously referred to as *petit mal*, nowadays childhood absence epilepsy (AE). Recent analysis on dynamics of cortical spreading in cerebral cortex during the initiation of SWDs in the WAG/Rij rat model for AE [10, 49] suggested an initial leading role of the cortex initiating SWDs and subsequently paroxysmal oscillations within cortico-thalamo-cortical loops, making it a unified oscillatory network; the thalamus sustaining and amplifying the discharge [28, 29]. For the first 500 ms of the generalization, a cortical zone was found to lead the thalamus [28]. Also, in another genetic rat absence model-GAERS, rhythmic burst firing in the deep subgranual cortical layers preceded the onset of SWDs, as could be recorded with local field potentials [38]. These studies suggest a cortical focal precursor for AE in genetic animal models. In humans, preliminary evidence for cortical and maximally frontal cortical involvement in AE has been shown with EEG [17, 48, 52], single photon emission computed tomography [21], and MEG [1, 2, 53]. These reports support the hypothesis that human SWDs might have localized precursors as well, rather than being a sudden generalized synchronous event. The localization of such cortical

precursors can be of much benefit in future therapeutic interventions for predicting or controlling the generalized discharges.

Nowadays, a popular hypothesis for cortical epileptic seizure precursors is [24]: during the interictal (seizure-free) state, the neuron populations around the epileptic focus are involved in large-scale dynamics of normal brain functioning. During preictal (preseizure) state, these neurons lose the synchronization with nearby cortical areas. This possibly isolates the epileptic focus from the normal brain networks and facilitates the development of a hyper-excitable focus. This also provides an 'idle' population of neurons that can be easily recruited by the focus. Seizure activity may then get initiated when a critical mass of neurons gets recruited. This indicates that precursors could be marked by decrease in local connectivity with a subsequent increase with seizure onset. Attempts have been made to measure such transitions from interictal to preictal state with various nonlinear methods, because ongoing clinical research suggests that pathological states such as seizures [3] have a strong nonlinear component. In general, for epileptic seizures a decrease in complexity [25], chaos [18], accumulated energy [26], and phase synchrony [31, 32] has been shown for varying amounts of preictal times (seconds to hours). For absence seizures in particular, bifurcation analysis [5, 6], phase synchrony [2, 11, 19, 35], and synchronization likelihood [46] have been applied, along with source imaging [2], to explore the network dynamics. These studies have explored the cortical interactions based on broad and narrow frequency bands. They commonly show interplay of local and long-range synchronization phenomena reproducible with a localized network.

The aim of this study is to extract preictal focal sources that recur in absence seizures, within a selected preictal time length. The analysis has been performed with MEG signals as they provide higher spatial resolution as compared to EEG and also have the advantage that the neuromagnetic fields are largely unaffected by in-homogeneities in the skull and the scalp [9]. We describe two methods that were applied separately: (1) nonlinear association (NA) analysis to resolve the transitions from interictal to preictal and ictal state applied within the framework of graph theory, and (2) time–frequency analysis (TFR) and coherence that reflect spectral connectivity with subsequent cortical source reconstruction during the transition from the interictal to the preictal and ictal state. We opt for the NA analysis, as it is a powerful technique to assess the evolvement of nonlinear dependencies in signals with the use of moving windows [37]. NA has been previously used in WAG/Rij rat data by Meeren et al. [28] and in MEG data by Westmijse et al. [53]. TFR and coherence are estimated with multitaper Fourier Transforms (mFT)

that is optimal for spectral estimation over a range of frequencies [30]. For cortical source reconstruction we applied Dynamic Imaging of Coherent Sources (DICS)—an adaptive frequency domain beamformer [7, 8, 13, 22, 23, 27, 42], mainly because DICS can be combined with spectral estimation over frequency bands of interest and it is also better equipped to handle the extraction of distinct sources that are in the vicinity of each other and are coherent in their activity [15].

2 Methods

2.1 Patients

Patients and data acquisition were identical to those described in the study of Westmijse et al. [53]. Briefly, five patients with absence epilepsy were included in this study, according to the criteria for absence epilepsy of the International League against Epilepsy (ILAE). These criteria were: (1) 3 Hz SWDs in the EEG with a minimum of 4 s, (2) impairment of consciousness, (3) no other seizure types present (either at the time of measuring or in history, with the exception of febrile seizures), (4) not being seizure-free at the time of measurement (medication was allowed), (5) no major myoclonic elements present during seizures, (6) normal neurologic development, and (7) the mental and physical ability to participate in the measurements. All patients (mean age 9.5, range 7–12 years) had a history of subsequently used different antiepileptic drugs (AEDs), but were not seizure-free at the time of measurement. After approval of the Committee for Research in Humans, written informed consent for the recordings was obtained from the parents of the patients, and in the case of the 12-year old also from herself.

2.2 MEG recordings

The MEG measurements were performed at the FC Donders Center for Cognitive Neuroimaging in Nijmegen, Netherlands. The MEG system used is the whole head system, with 151 sensors in the first four patients and 275 sensors in patient 5 (CTF Systems Inc., VSM MedTech Ltd., Coquitlam, BC, Canada). The anti-aliasing filter of the CTF hardware system was set to 300 Hz and the sampling frequency of the data was 1200 Hz. All patients were measured in a supine position. Patients received a three-dimensional (3D) MRI (MPRAGE sequence with 1 mm isotropic resolution; Siemens, Erlangen, Germany), in order to relate the functional (MEG) data to the anatomy of the individual patient. The three reference points (left and right pre-auricular points and the nasion) of the revised

combinatorial nomenclature system were used to co-register the functional and anatomical data.

2.3 MEG analysis

The first method in this analysis is to ascertain the existence of significant (compared to baseline) nonlinear interactions between various areas of the brain. We used the NA analysis for this purpose, as performed by Westmijse et al. [53], on the same datasets, for 5 s long MEG time segments (1 s preictal and 4 s ictal data) for all channels across all seizures. Subsequently followed by visualizing the dynamics of NA interactions prior to and during SWD onset with network parameters obtained from graph theory [4]. A separate frequency-domain coherence connectivity analysis with subsequent cortical source reconstruction with DICS beamforming [13, 16, 39] is applied to localize the source activity apparent during SWD onset. The data analysis was performed with the Fieldtrip open source toolbox [12].

2.4 Temporal network connectivity

NA was used to measure linear as well as nonlinear interactions between all possible pairs of brain signals with moving window of 187.5 ms shifted at 20 ms (the optimization of the window length and overlapping has been explained in [53]). The metric used for investigating the network parameters is the clustering coefficient (CC), defined as the mean clustering across a data segment across all nodes in the network [44]. It is a measure of local interconnectedness in a graph. In this case the 'nodes' are represented by the MEG sensors and the 'degree' by the average number of interactions or connections between all possible pair-wise combinations of MEG sensors, within a data segment of 187.5 ms. In addition, the path length which is defined as the characteristic path length (CPL) is used [45, 47]. The CPL is defined as the mean of all shortest paths between all pairs of nodes. It is a measure of global connectivity. An ordered graph has a high CC and a high CPL, while a random graph has a low CC and a low CPL. Whereas a graph that shows small world properties has a high CC but a low CPL. To ensure for significance, we normalize the CC and CPL by the average CC′ and CPL′ values of 100 surrogate random graphs. In addition to these metrics, the relationship between the local connectedness and the global integration of a network can also be described by its 'small worldness' (S), given by the ratio of normalized CC and CPL values. S > 1 shows in effect a CC > CPL. The significance of the normalized CC and CPL values compared to interictal is ensured by comparing it against the CC and CPL value distribution of 25 concatenated random interictal MEG signal segments of the same length (187.5 ms).

2.5 Spatial–spectral connectivity

The spectral power for TFR is estimated with mFT, across frequency bands of 0–50 Hz for all channels across all seizures. The time–frequency representation (TFR) of power is calculated using a sliding (overlapped) time window of 50 ms (1/10 of the time length at which connectivity transitions were observed in rats [28]). The time windows used here decrease in length with increased frequency, where power is calculated for each time window. This allows higher temporal resolution with increasing frequency, although at an expense of reduced frequency resolution. The power value is assigned to the central time point of the time window. The temporal evolution of power values for each frequency is then expressed as the relative increase or decrease with respect to the power in the interictal period (prior to the preictal period). Figure 1b is shown as an example of the temporal evolution of power of the MEG data of patient 2 (Fig. 1a). The TFR maps across time show that the low frequency band (2–4 Hz) and high frequency bands (20–25 Hz) reflect maximal alteration from the control period, across the datasets. We investigate further the low frequency band, as it is relevant to the 3 Hz SWDs that follow the preictal state and a possible transition to a similar slow activity is more plausible for the identification of a focal precursor. For patient 2 the TFR analysis, frequency band of 2–4 Hz, power, relative to interictal, was observed to increase locally in the frontal and in the occipital regions during the 500 ms prior to the first generalized spike (FGS) (Fig. 1c). Next the cross-spectral density (CSD) matrices for the 2–4 Hz bands of all possible pairs of MEG channels at the selected frequency band of interest is computed. The CSD matrix is computed from the Fourier transforms (FT) of the data by multiplying the FT of one signal with the complex conjugate of the other signal. The diagonal of the CSD matrix gives the power spectrum of the signal. Coherence is estimated by normalizing the magnitude of the summed cross-spectral density between two signals by their respective powers. Selecting the frontal channels as the region of interest (ROI) for patient 2 shows the dynamics of spectral connectivity of the frontal region with the occipital and neighboring frontal regions (Fig. 1d).

The CSD matrices obtained above are also used for subsequent beamforming for a high spatial resolution of signal variance. Beamforming essentially aims to pass signals from a location of interest while blocking signals from all other locations. Its main operator is the weight vector that when applied to the MEG data gives a scan

Fig. 1 a MEG channel data for patient 2. The channel names indicate *M* MEG, *L* left, *F* frontal, *C* central. **b** Power estimates for the beamformed sources. Power is observed to increase at 3 s. **c** Time frequency topographies relative to interictal periods. The range for all maps is fixed. Frontal activity along with occipital activity is observed to evolve and increase in strength by 3.2 s. **d** Coherence topographies for 2–4 Hz, with reference to a left frontal ROI. Connectivity with occipital region is observed at around 3 s. **e** Beamformed sources projected on to the volumetric anatomical data with patient specific MRI
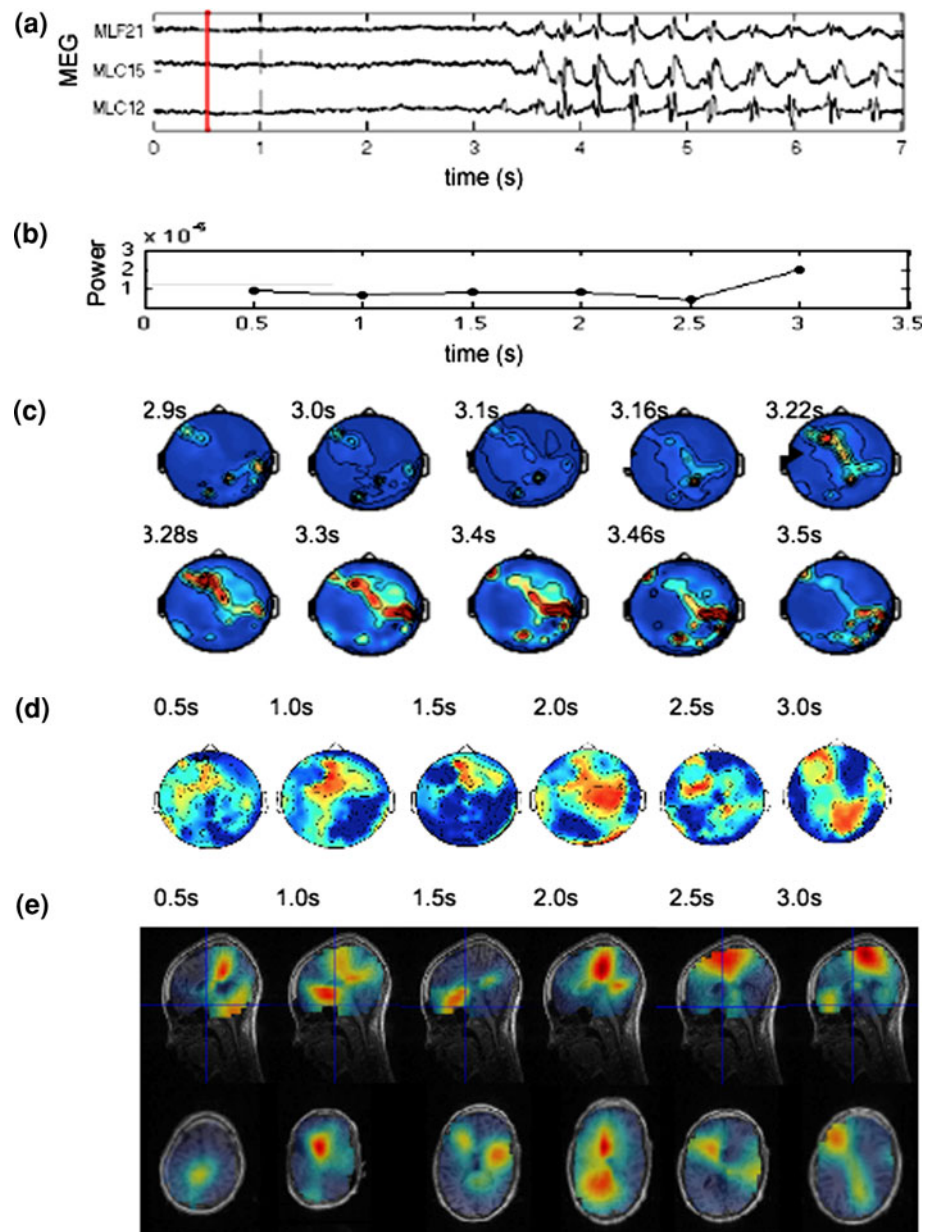
metric value potentially estimating dipole source activity at a particular location. A full attenuation of sources outside the location is not possible, therefore an optimal solution is to minimize the contribution of those sources or in other words minimize the variance of the beamformer output. The weight vector (or more commonly referred to as the spatial filter) is computed from the lead field (forward model estimation of the field measured by the MEG sensors corresponding to a dipole of unit moment) of a location and the CSD matrix. We overcome possible numerical instability of the CSD matrix by a regularization of 0.01%. Low regularization values (<1%) have been shown to make the spatial filter more spatially selective and resulting in substantial suppression of artifacts [27]. We circumvent

the bias of the CSD spatial filters to attribute more power to deep sources, by computing the Neural Activity Index (NAI). NAI is the power normalized with an estimate of the uncorrelated spatially inhomogeneous noise estimated on the basis of the smallest Eigen value of the CSD matrix [30].

DICS was then used to localize the time varying sources in the low frequency domain using a time window of ±285 ms long (low temporal resolution for low frequency) (Fig. 1e). To obtain the functional image, the required number of weight vectors is equal to the number of voxels (locations) in the brain volumetric image. Voxels are obtained by segmenting the brain surface from patient MRI, followed by discretizing the volume (using a semi-

realistic head model developed by Nolte [33]) into a 3D grid, with a 1 cm resolution. As mentioned above, the per-voxel spatial filter is then applied to the FT of the data adaptively attempting to fit the unconstrained dipole sources in the selected frequency band at each voxel in the brain volume. The results of the source strength estimation are superimposed on the anatomical MRI. The alignment of the MRI and functional data is performed according to the anatomical landmarks: the three fiducial points: nasion, preauricular left, and preauricular right, that are both determined in the brain activity measurement and in the MRI scan. The results are also projected on to the brain surface (in MNI coordinates); by normalizing the volume to match those coordinates.

3 Results

3.1 Clustering

NA connectivity information is used to examine the dynamics of connectivity as the brain transits from inter-ictal to preictal and ictal state. Network connectivity was determined in two ways (Fig. 2): (1) by using a threshold based on the maximal number of connections during the interictal state; and (2) by using an optimal threshold based on the strength of the connectivity. A constant number of connections or constant node degree for increasing thresholds (Fig. 2i) reveals a clear distinction in behavior of the interictal, preictal, and ictal states. It shows firstly that interictal segments can generally have the same number of average connections (degree) as the ictal segments at low thresholds (<10). Secondly, Fig. 2i shows also that the degree in ictal segments tends to be higher than that of preictal and interictal segments at higher (>50) thresholds. Moreover, at the time of the SWDs during the ictal period, the degree is the highest. For example, the average number of connections at threshold 50 is 24 for interictal segments, 78 for preictal, and 131 for ictal segments.

To further examine the preictal and ictal local and global clustering effects, an *optimal threshold* value for the NA interactions was determined. The optimal threshold in this case sets apart the interictal from the preictal and ictal periods. This has been computed for each patient, by obtaining the mean CC across all the time windows of the interictal segments, at each threshold (Fig. 2ii) and the mean CC across all time windows within the preictal and ictal segments, at each threshold (Fig. 2iii). Normalizing the mean preictal plus ictal CCs across thresholds with the respective interictal mean CCs (Fig. 2iv) shows a transition point, indicating the threshold level at which the preictal plus ictal mean connectivity supersedes the interictal

connectivity strength. This threshold value obtained for each seizure of the five patients has been used for further analysis of the global and local preictal plus ictal connectivity of the network underlying SWDs.

3.2 Small world networks

For the computation of the small world network (SWN) indices we used the information that the interictal and preictal plus ictal states tend to have the same maximum degree at a threshold of 10 and up to 30, respectively. Clustering indices are computed at these thresholds and averaged across seizures and five patients. Figure 3(i) shows, from top to bottom, the averages (and standard deviations) of the local clustering (CC), the global clustering (CPL), the normalized local and global clustering and the measure for *small worldness* (S = CC/CPL). The vertical blue line indicates the clinician's marker for onset. Both the local and global clustering show a distinct transition at the seizure onset marker, with the CC remaining at the higher level and the CPL at a lower level throughout the ictal as compared to the interictal period. The combination of the normalized CC and CPL shows the increase in CC and decrease in CPL from the seizure onset marker onwards. This indicates the tendency to a SWN after the transition point at the seizure onset marker. Further, the results shown at the bottom of Fig. 3(i) clearly indicate a higher S for ictal segments as compared to the precursor segments. It is interesting to note that the preictal segments show a relatively higher local clustering of approximately 0.9 indicating local clusters albeit with weaker connectivity's compared to ictal.

In Fig. 3(ii) the local and global connectivity indices at the optimal threshold as determined in Fig. 2iv are shown for one seizure of each patient. A general sharp increase in local connectivity (CC) and decrease in global connectivity (CPL) is observed across all patients at the seizure onset marker. Another interesting observation is the trend of connectivity during seizure propagation. The rhythmic pattern of peaks and troughs corresponding with the occurrences of spikes and waves in the MEG signal show the increasing and decreasing connectivity across time which is in concordance with the findings of Westmijse et al. [53], where a large-scale cortical generalization (during waves) was observed in points with high association values to be followed by focal clusters at the time of spikes throughout the ictal period. The CC, CPL connectivity results in this case (connectivity at higher strength) were not averaged across seizures and patients to preserve the rhythmic morphology which is easily lost, when the spike and wave events do not overlap in time for each seizure and patient.

Fig. 2 i Shown for one example patient is: the average number of connections per channel (degree) (*y*-axis) versus the threshold (*x*-axis). Each *curve* represents a 187.5 ms segment centered at the time shown in the legend, during interictal, preictal and ictal periods and ictal periods including intervals with spikes. **ii** Mean of CC across time for concatenated interictal segments at varying thresholds. **iii** Mean of CC across time for each of the ictal segments at varying thresholds. Each *curve* represents a seizure; each marker type represents a patient. **iv** Mean CC ictal relative to the mean CC interictal at varying thresholds for two seizures each of all patients. Mean normalized CC shows the threshold deflection point after which the clustering for ictal segment exceeds that of interictal segments
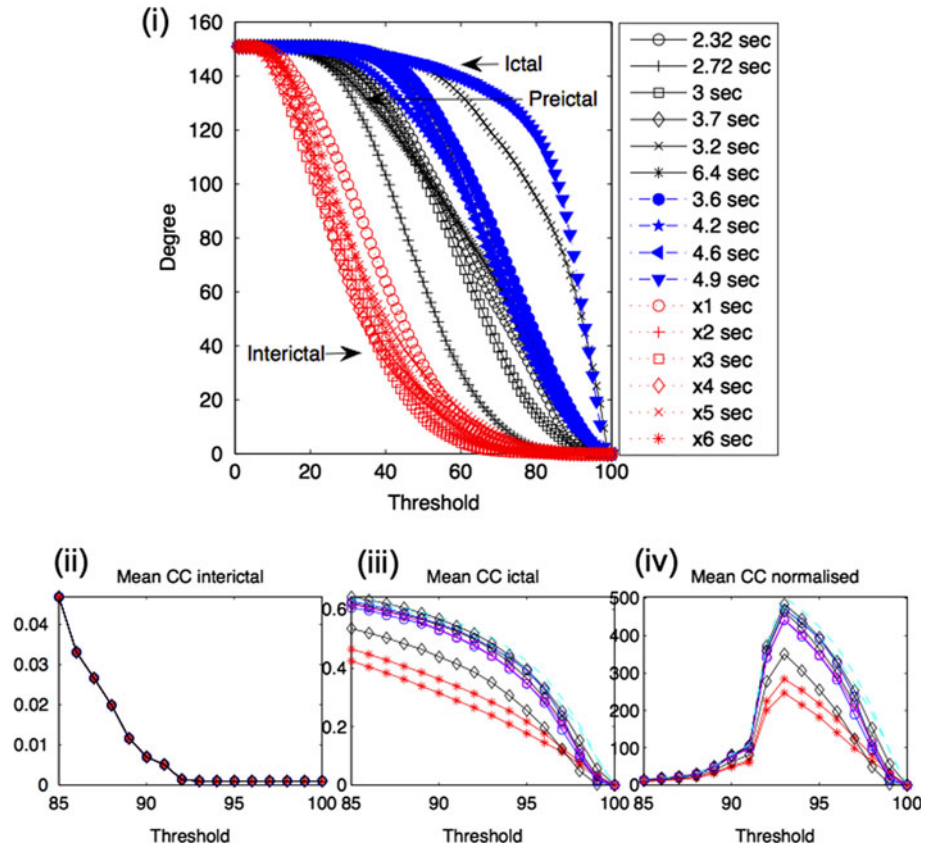
Fig. 3 i Local connectivity (CC), global connectivity (CPL), normalized CC and CPL, and 'small worldness' (S = CC/CPL) averaged across 9 seizures of five patients (*solid dark lines*) versus the same graphs for random interictal segments (*red dashed lines*). Standard deviation (*dotted dark*) for the ictal segments across patients is shown along the average CC and CPL. **ii** CC, CPL for a representative seizure of the five patients separately, illustrating the connectivity changes at seizure onset, followed by a rhythmic pattern of high and low connections during seizure propagation. The *vertical blue line* marks the seizure onset marked by clinicians
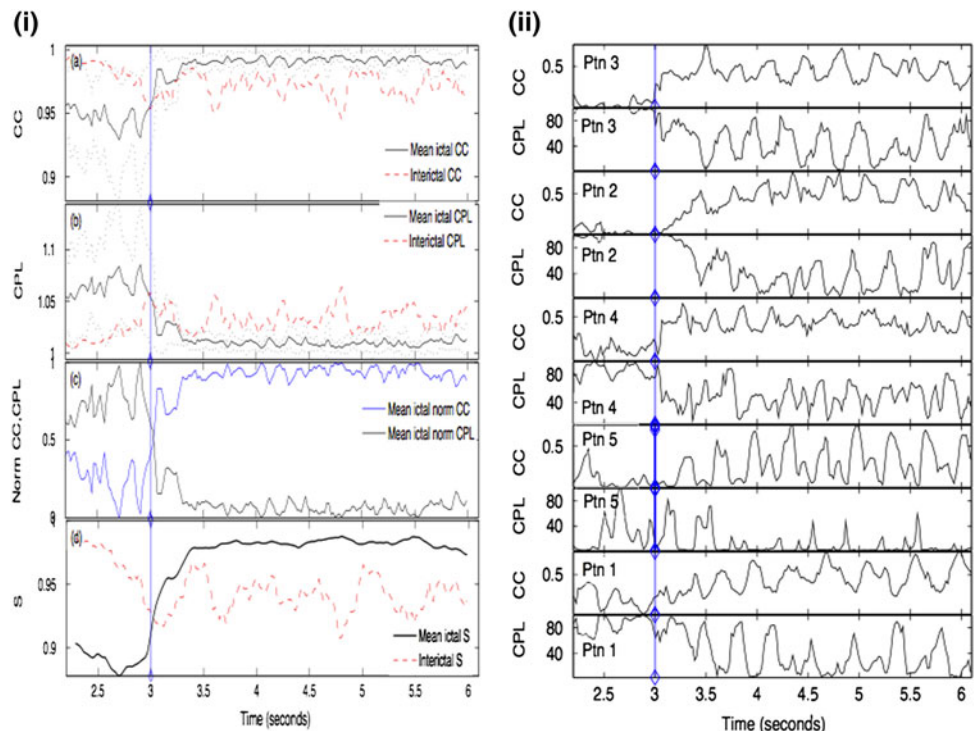
3.3 Source analysis

In order to identify the source activity in the transition period from interictal to preictal and ictal state the frequency-domain coherence connectivity analysis with subsequent cortical source reconstruction using DICS beamforming as illustrated in Fig. 1 was applied for all seizures across the five patients. The results were obtained for the 2–4 Hz frequency band (fc = 3 Hz) and the data used in computing each source is a 1 s segment. As an example the results of one of the patients (patient 1) are shown in Fig. 4. The MEG data are shown (upper row) from 3 s before the first visible onset of the SWDs, the marker placed by the clinician, and 4 s after the marker. Indicated in these signals is a time window of (source) analysis with the midpoint of the interval (red cursor) either preceding the marker (left) or subsequent to the marker (right), for seizure 1 and seizure 2. The beamforming results for each of the time windows are plotted at a sagittal and axial MR scan, and according to the dominant strength distribution projected at a tilted 3D rendering of the patients cortex. These results indicate for patient 1, maximal occipital source activity in the time window preceding seizure onset and maximal frontal source activity in the time window after seizure onset, prior to the FGS.

The results of DICS shown for patient 2–5 consistently show a low power occipital source becoming apparent prior to the seizure onset marker (Fig. 5, left column) and a frontal source becoming apparent in the time frame following the seizure onset, again prior to the FGS

(Fig. 5, right). Note, furthermore, that the beamforming results are quite consistent for both of the seizures of patient 1, 2, 3, and 5. There was only one seizure obtained for patient 4. As expected, a slight shift in time can be observed in the occurrence of maximal source activity for each patient. Incidentally, the source activity also reflects a corresponding transient source in the fronto-temporal region. For patient 1, for example, maximal temporal source activity corresponds to the occurrence of the frontal source (see Fig. 4, right column), however, for patient 2, 3, and 4 temporal source activity mainly becomes apparent during the occurrence of the occipital source.

4 Discussion

The aim of this study was to describe the spatial and temporal profiles of cortical networks and sources within the framework of graph theory during the evolvement of MEG SWDs typical for childhood AE. According to the classification of the ILAE, these SWDs occur abruptly as bilaterally synchronous generalized discharges. However, the results of this study show that before the first generalized discharges in the so-called ictal state, a preictal period can be distinguished with a clear onset becoming apparent with a transition from an interictal to a preictal state. Note that this transition point corresponds closely to the clinician's marker at the first visible onset of the SWDs. Furthermore, the time–frequency source analysis performed for the AE data across the five patients consistently
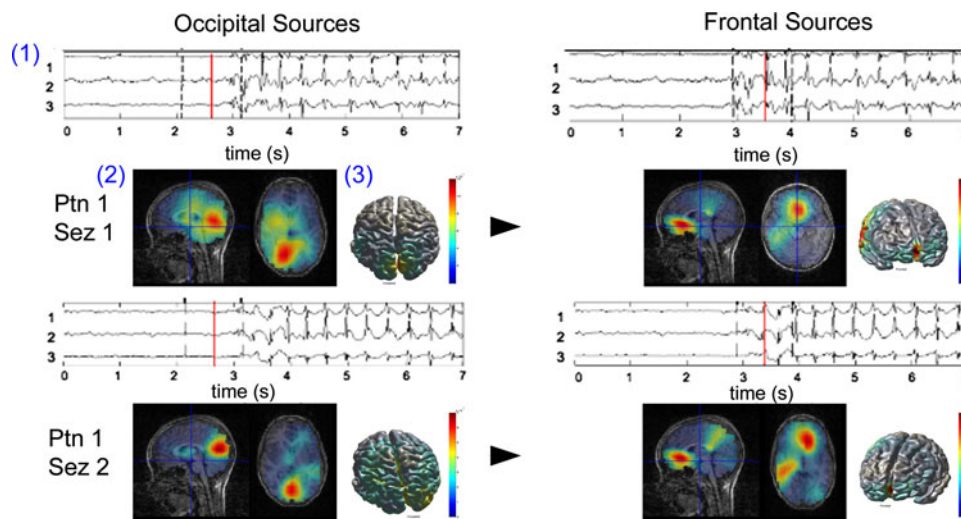
Fig. 4 Shown is the output of DICS for the two seizures of patient 1. Per seizure are depicted: **1** the MEG signals (the 3 s mark is the first visible onset as marked by the clinician). The *dashed vertical lines* mark the window of data used for low frequency beamforming and the *red vertical line* marks the center of that data window. **2**, **3** The sagittal and axial view and the cortical surface (rotated for best view)

plot of the beamformed source(s). To provide a spatial frame of reference, cross hairs mark the same fixed point on all sagittal scans; the axial scans are plotted with the nose up. The *left column* reflects the occipital sources occurring approximately 1 s before the transient frontal source (*right column*) evolves at or prior to the first generalized spike of the SWD

Fig. 5 The output of DICS for two seizures for patient 2, 3, and 5, and for one seizure for patient 4, plotted using the same conventions as in Fig. 4 for patient 1 (see Fig. 4 legend for further details)
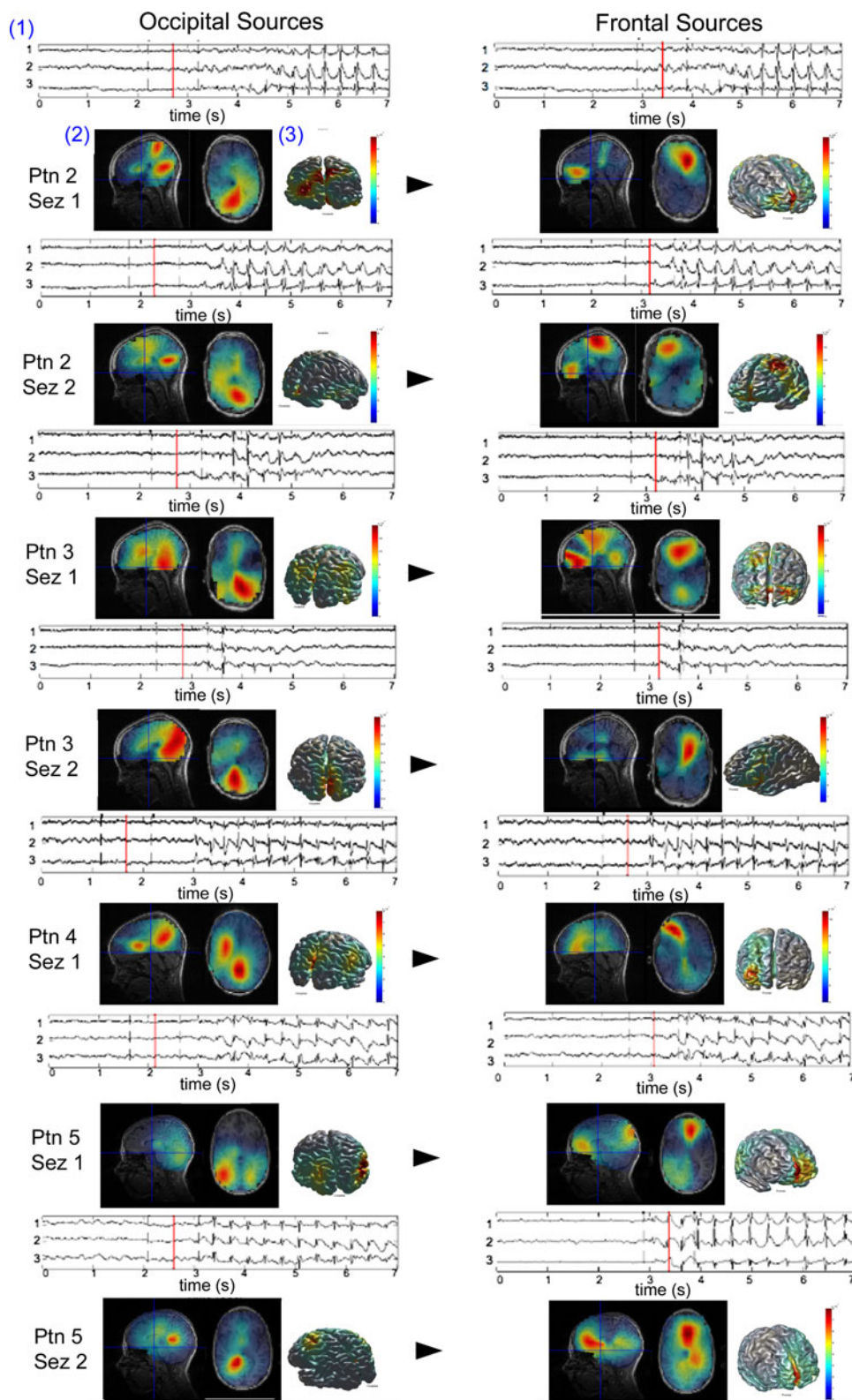
showed that the source activity in the preictal period prior to the FGS converged onto frontal cortical areas. These sources found for the low frequency band (fc = 3 Hz) are in accordance with the frontal onset of the SWDs as indicated by the NA analysis results [53]. However, since we were interested, especially, in source activity occurring prior to the first visible onset and the subsequent seizure discharge, the time–frequency source analysis was

performed in an interval preceding the clinicians marker with approximately 1 s. The results of this analysis consistently showed across the five patients a low power (fc = 3 Hz) occipital source preceding/evolving along the rapidly evolving source in the frontal cortex. Interestingly, genetic epileptic WAG/Rij rats have also clear low frequency delta activity prior to the onset of SWDs in cortex and thalamus [50]; it is also likely that synchronized activity in cortex and thalamus builds up or reduces before SWD onset, rather than being a sudden generalized synchronous event. The latter has also been proposed in WAG/Rij rats based on outcomes of classical FFTs, NA analyses, and wavelet analyses [14, 28, 43]. However, the current study is a preliminary study and it needs to be assessed with a larger data set. Moreover, further analysis in the higher frequency band will add to our findings where frontal and parietal sources at the time of spikes and waves were observed during the seizure propagation using a SAM beamformer (for frequencies >20 Hz), for the same dataset [53]. Scalp EEG recordings with a high degree of spatio-temporal resolution, in combination with source analysis and a realistic MRI model, demonstrated that localized orbitofrontal and medial frontal, and occasionally temporal regions were most commonly involved at the onset and in the propagation of ictal discharges in absences [17, 48]. For source analysis of either EEG or MEG epileptic data equivalent dipole modeling [34, 40] or models that reflect distributed source activity, like amongst others LORETA [36] or minimum variance spatial filters [51] can be used. We used, however, a DICS beamformer which is well suited for the detection of spatially close sources in the time domain and focused on low frequencies, which confirmed the important role of the frontal cortex and found, not previously described, preictal occipital sources.

The occipital precursor activity was not only determined qualitatively in this study by putting a marker at the first visible onset, but also quantitatively by determining the transition point from the interictal to the ictal interval. This transition point was reflected in a sudden increase versus decrease of the local and global CCs across seizures of the five patients studied. It is important to note that in the clustering analysis, a subtle bias can creep in with regards to the strength of connectivity at interictal versus ictal periods. A preselected "degree" or threshold is used usually to assess the local and global connectivity across brain activity. Computing the clustering with the use of the same threshold for connectivity during interictal and ictal periods may not be the correct assessment of emergence or disruption of clustering in the network. It can be assumed that there is always some connectivity interictally. To remove this bias and to truly measure if the transition involves increasing clustering, irrespective of the scale of association, the threshold for a time window should be based on a constant

degree (average number of connections per channel) during the interictal and ictal segments. However, it can also be informative to study the dynamics in the clustering patterns irrespective of the connectivity strength. Therefore, we studied the network connectivity in two ways (see Fig. 2): by using a threshold based on the maximal number of connections during the interictal states and with optimal threshold based on strength of connectivity. A further analysis of ictal clustering at higher strength of connectivity can then be performed at the thresholds at which the degree for the interictal segment diminishes.

Another important aspect observed is the tendency towards a SWN observed prior to the SWD. An increase in clustering index and decrease in the CPL across the patients and seizures showed the tendency towards a SWN from approximately 1 s before the FGS occurred. The emergence of a SWN with the onset of SWDs may suggest a pathologically predisposed state towards synchronous seizure networks with increasing connectivity from preictal to ictal state. This corresponds to the findings about a general reduction in SWN characteristics and increase in randomness related to activity of a brain with a functional disorder as shown for Alzheimer disease [47] and in schizophrenic patients [41]. In the same context it may be hypothesized that the epileptic brain has a generally lower CC and CPL (increased randomness) (which also makes it more susceptible to seizures) and transitions to a small world like network on seizure onset in an attempt to increase order. However, our findings when observed in the context of interictal to preictal to ictal state may also indicate a transitory preictal state stretching over a longer time span than 1 s. Such a preictal phase may confirm the general seizure prediction hypothesis of decreased synchrony, chaos, or complexity that marks preseizure activity. A preictal state with reduced local connectivity's and higher global connections might suggest a phase where the inhibitory network strengthens and a focus gets briefly isolated from normal brain processes, subsequently rapidly recruiting networks for SWDs.

References

1. Amor F, Rudrauf D, Navarro V, N'diaye K, Garnero L, Martinerie J, Le Van Quyen M (2005) Imaging brain synchrony at high spatio-temporal resolution: application to MEG signals during absence seizures. Signal Process 85:2101–2111

2. Amor F, Baillet S, Navarro V, Adam C, Martinerie J, Le Van Quyen M (2009) Cortical local and long-range synchronization

interplay in human absence seizure initiation. NeuroImage 45:950–962

3. Andrezejak RG, Laehnertz K, Mormann F, Rieke C, David P, Elger CE (2001) Indications of nonlinear deterministic and finite-dimensional structure in time series of brain electrical activity: dependence on recording region and brain state. Phys Rev E 64:061907

4. Bassett DS, Bullmore E (2006) Small-world brain networks. Neuroscientist 12:512–523

5. Breakspear M (2004) Dynamic connectivity in neural systems. NeuroInformatics 2:205–224

6. Breakspear M, Roberts JA, Terry JR, Rodrigues S, Mahant N, Robinson PA (2006) A unifying explanation of primary generalized seizures through nonlinear brain modeling and bifurcation analysis. Cereb Cortex 16:1296–1313

7. Canolty RT, Edwards E, Dalal SS, Soltani M, Nagarajan SS, Kirsch HE, Berger MS, Barbaro NM, Knight RT (2006) High gamma power is phase-locked to theta oscillations in human neocortex. Science 313:1626–1628

8. Dalal SS, Guggisberg AG, Edwards E, Sekihara K, Findlay AM, Canolty RT, Berger MS, Knight RT, Barbaro NM, Kirsch HE, Nagarajan SS (2008) Five-dimensional neuroimaging: localization of the time–frequency dynamics of cortical activity. Neuroimage 40:1686–1700

9. de Jongh A, de Munck JC, Gonçalves SI, Ossenblok P (2005) Differences in MEG/EEG epileptic spike yields explained by regional differences in signal-to-noise ratios. J Clin Neurophysiol 22:153–158

10. Depaulis A, van Luijtelaar G (2006) Genetic models of absence epilepsy in the rat. In: Pitkänen A, Schwartzkroin F, Moshe S (eds) Models of seizures and epilepsy. Elsevier, Amsterdam, pp 233–248

11. Dominguez LG, Wennberg RA, Gaetz W, Cheyne D, Snead OC, Velazquez JLP (2005) Enhanced synchrony in epileptiform activity? Local versus distant phase synchronization in generalized seizures. J Neurosci 25:8077–8084

12. Fieldtrip open source toolbox for Neuroimaging: http://www.ru.nl/neuroimaging/fieldtrip. Donders Centre for Cognitive Neuroimaging, Radboud University Nijmegen, Nijmegen, the Netherlands

13. Gross J, Kujala J, Hämäläinen M, Timmermann L, Schnitzler A, Salmelin R (2001) Dynamic imaging of coherent sources: Studying neural interactions in the human brain. Proc Natl Acad Sci USA 98:694–699

14. Gurbanova AA, Aker R, Sirvanci S, Demiralp T, Onat FY (2008) Intra-amygdaloid injection of kainic acid in rats with genetic absence epilepsy: the relationship of typical absence epilepsy and temporal lobe epilepsy. J Neurosci 28:7828–7836

15. Hadjipapas A, Hillebrand A, Holliday IE, Singh KD, Barnes GR (2005) Assessing intersections of linear and non-linear neuronal sources using MEG beamformers: a proof of concept. Clin Neurophysiol 116:1300–1313

16. Hamalainen MS, Ilmoniemi RJ (1984) Interpreting measured magnetic fields of the brain: estimates of current distributions, Helsinki Univ. of Tech., Finland, TReport TKKK-F-A599

17. Holmes M, Brown M, Tucker D (2004) Are 'generalized' seizures truly generalized? Evidence of localized medial frontal and frontopolar discharges in absence. Epilepsia 45:1568–1579

18. Iasemidis LD, Sackellare JC (1996) Review: chaos theory and epilepsy. Neuroscientist 2:118–126

19. Inouye T, Sakamoto H, Shinosaki K, Toi S, Ukai S (1990) Analysis of rapidly changing EEGs before generalized spike and wave complexes. Electroencephalogr Clin Neurophysiol 76:205–221

20. Jasper HH, Kershman J (1941) Electroencephalographic classification of the epilepsies. Arch Neurol Psychiatry 45:903–943

21. Kapucu LO, Serdaroglu A, Okuyaz C, Kose G, Gucuyener K (2003) Brain single photon emission computed tomographic evaluation of patients with childhood absence epilepsy. J Child Neurol 18:542–548

22. Kujala J (2008) Study of cortical rhythmic activity and connectivity with magnetoencephalography. PhD thesis, Helsinki University of Technology

23. Kujala J, Gross J, Salmelin R (2008) Localization of correlated network activity at the cortical level with MEG. NeuroImage 39:1706–1720

24. Le Van Quyen M (2005) Anticipating epileptic seizures: from mathematics to clinical applications. C R Biol 328:187–198

25. Lehnertz K, Elger CE (1995) Spatio-temporal dynamics of the primary epileptogenic area in temporal lobe epilepsy characterized by neuronal complexity loss. Electroencephalogr Clin Neurophysiol 95:108–117

26. Lehnertz K, Mormann F, Kreuz T, Andrzejak RG, Rieke C, David P, Elger CE (2003) Seizure prediction by nonlinear EEG analysis. IEEE Eng Med Biol 22:57–63

27. Litvak V, Eusebio A, Jha A, Oostenveld R, Barnes GR, Penny WD, Zrinzo L, Hariz MI, Limousin P, Friston KJ, Brown P (2010) Optimized beamforming for simultaneous MEG and intracranial local field potential recordings in deep brain stimulation patients. Neuroimage 50:1578–1588

28. Meeren HKM, Pijn JPM, van Luijtelaar ELJM, Coenen AML, Lopes da Silva FH (2002) Cortical focus drives widespread corticothalamic networks during spontaneous absence seizures in rats. J Neurosci 22:1480–1495

29. Meeren H, van Luijtelaar G, Lopes da Silva F, Coenen A (2005) Evolving concepts on the pathophysiology of absence seizures the cortical focus theory. Arch Neurol 62:25–37

30. Mitra PP, Pesaran B (1999) Analysis of dynamic brain imaging data. Biophys J 76:691–708

31. Mormann F, Andrzejak RG, Kreuz T, Rieke C, David P, Elger CE, Lehnertz K (2003) Automated preictal state detection based on a decrease in synchronization in intracranial electroencephalography recordings from epilepsy patients. Phys Rev E 67:021912

32. Mormann F, Kreuz T, Andrzejak RG, David P, Lehnertz K, Elger CE (2003) Epileptic seizures are preceded by a decrease in synchronization. Epilepsy Res 53:173–185

33. Nolte G (2003) The magnetic lead field theorem in the quasi-static approximation and its use for magnetoencephalography forward calculation in realistic volume conductors. Phys Med Biol 48:3637–3652

34. Ossenblok P, de Munck JC, Colon A, Drolsbach W, Boon P (2007) Magnetoencephalography is more successful for screening and localizing frontal lobe epilepsy than electroencephalography. Epilepsia 48:2139–2149

35. Palva JM, Palva S, Kaila K (2005) Phase synchrony among neuronal oscillations in the human cortex. J Neurosci 25:3962–3972

36. Pascal-Marqui RD, Michel CM, Lehmann D (1994) Low resolution electromagnetic tomography, a new method for localizing electrical activity in the brain. Int J Psychophysiol 18:49–65

37. Pijn JPM (1990) Quantitative evaluation of EEG signals in epilepsy: nonlinear associations time delays and nonlinear dynamics. University of Amsterdam, Netherlands

38. Polack PO, Guillemain I, Hu E, Deransart C, Depaulis A, Charpier S (2007) Deep layer somatosensory cortical neurons initiate spike-and-wave discharges in a genetic model of absence seizures. J Neurosci 27:6590–6599

39. Quraan MA, Moses SN, Hung Y, Mills T, Taylor MJ (2010) Detection and localization of hippocampal activity using beamformers with MEG: a detailed investigation using simulations and empirical data. Human Brain Mapping, n/a. doi:10.1002/hbm.21068

40. Rodin E, Rodin M, Thompson J (1994) Source analysis of generalized spike–wave complexes. Brain Topogr 7:113–119

41. Rubinov M, Knock SA, Stam CJ, Micheloyannis S, Harris AW, Williams LM, Breakspear M (2009) Small-world properties of nonlinear brain activity in schizophrenia. Hum Brain Mapp 30:403–416

42. Sekihara K, Nagarajan SS, Peoppel D, Marantz A, Miyashita Y (2001) Reconstructing spatio-temporal activities of neural sources using an MEG vector beamformer technique. IEEE Trans Biomed Eng 48:760–771

43. Sitnikova E, van Luijtelaar G (2009) Electroencephalographic precursors of spike-wave discharges in a genetic rat model of absence epilepsy: power spectrum and coherence EEG analyses. Epilepsy Res 84:159–171

44. Soffer SN, Vázquez A (2005) Network clustering coefficient without degree-correlation biases. Phys Rev E Stat Nonlin Soft Matter Phys 71(5 Pt 2):057101

45. Stam CJ (2004) Functional connectivity patterns of human magnetoencephalographic recordings: a 'small-world' network? Neurosci Lett 355:25–28

46. Stam C, van Dijk B (2002) Synchronization likelihood: an unbiased measure of generalized synchronization in multivariate data sets. Phys D: Nonlinear Phenom 163:236–251

47. Stam CJ, Jones BF, Nolte G, Breakspear M, Scheltens P (2007) Small-world networks and functional connectivity in Alzheimer's disease. Cereb Cortex 17:92–99

48. Tucker D, Brown M, Luu P, Holmes M (2007) Discharges in ventromedial frontal cortex during absence spells. Epilepsy Behav 11:546–557

49. van Luijtelaar G, Sitnikova E (2006) Global and focal aspects of absence epilepsy: the contribution of genetic models. Neurosci Biobehav Rev 30:983–1003

50. van Luijtelaar G, Hramov A, Sitnikova E, Koronovskii AA (2011) Spike-wave discharges in WAG/Rij rats are preceded by delta and theta precursor activity in cortex and thalamus. Clin Neurophysiol 122:687–695

51. van Veen BD, van Drongelen W, Yuchtman M, Suzuki A (1997) Localization of brain electrical activity visa linearly constrained minimum variance spatial filtering. IEEE Trans Biomed Eng 44:867–880

52. Vuilleumier P, Assal F, Blanke O, Jallon P (2000) Distinct behavioral and EEG topographic correlates of loss of consciousness in absences. Epilepsia 41:687–693

53. Westmijse I, Ossenblok P, Gunning B, van Luijtelaar G (2009) Onset and propagation of spike and slow wave discharges in human absence epilepsy: a MEG study. Epilepsia 50:2538–2548